Silica Nanoparticle Separation from Water by Aggregation with AlCl3

Yanping Liu, Mallorie Tourbin, Sebastien Lachaize, Pascal Guiraud

Silica Nanoparticle Separation from Water by Aggregation with $AlCl_3$

Yanping Liu,[†,‡,§] Mallorie Tourbin,[†,‡,§,#] Sébastien Lachaize,[∥,⊥] and Pascal Guiraud[*,†,‡,§]

[†]Université de Toulouse; INSA, UPS, INP; LISBP, 135 Avenue de Rangueil, F-31077 Toulouse, France

[‡]INRA, UMR792 Ingénierie des Systèmes Biologiques et des Procédés, F-31400 Toulouse, France

[§]CNRS, UMR5504, F-31400 Toulouse, France

[∥]Université de Toulouse; INSA, UPS; LPCNO, 135 avenue de Rangueil, F-31077 Toulouse, France

[⊥]CNRS, LPCNO, F-31077 Toulouse, France

ABSTRACT: Nanotechnology that is vigorously developed nowadays will inevitably let nanoparticles into water resources. Since these ultrasmall particles may have potential risks for human and animals, it is reasonable to consider urgently how to manage these polluted waters. The direct separation would be difficult due to their small size and high surface area, so $AlCl_3$ is added to modify surface physicochemical properities of nanosilica in order to produce aggregates. Early stages and long time equilibrium of nanosilica aggregation are explored. In the kinetics study (early stage), the influences of particle concentrations and particle sizes are studied and compared. The aggregation results at long time equilibrium are further investigated, which shows the charge neutralization effect could be overcome by other mechanisms. More than 99% of the turbidity can be removed from aggregation of nanosilica by $AlCl_3$ after sedimentation.

1. INTRODUCTION

Because of the vigorous development of nanotechnologies, the recovery of nanoparticles from wastewater to reinject cleaner water or from hydric resources to produce drinking water would be an important challenge in the near future. These particles may be found in the aquatic environment since industrial products and wastes tend to end up in waterways (e.g., drainage ditches, rivers, lakes, estuaries, and coastal waters) despite safeguards.[1,2] From accidental spillages or permitted release of industrial effluents, nanoparticles can be accumulated into the body via skin contact, inhalation of water aerosols, direct ingestion of contaminated drinking water, or indirect exposure from ingestion of vegetables and organisms such as fish, molluscs, and crustaceans as a part of the human diet.[2]

The potential hazards of nanoparticles are still largely unknown, even if hazards relevant to humans and animals health begin to be listed or investigated. Nanoaerosols seem to be the most toxic as it can enhance pulmonary pathologies, but specific hazards of nanoparticles have also been pointed out in aquatic environment.[3,4] Nanoparticles that are easily deteriorated into very low toxicity substances or excreted out of the biological tissues might be less dangerous than the biopersistent ones. Solubility, material toxicity, concentration, surface state, and shape of these particles seem to be important factors for the estimation of the actual risk.[5] Consequently, there has been little pressure to defense or manage wastewaters containing such particles that may present novel toxicity beyond those already existing by naturally occurring combustion products, volcanic ash, toxic metals, and organic xenobiotics. In fact, the very large surface area of ultrasmall particles can result in the direct generation of harmful oxyradicals (ROS): these can cause cell injury by attacking DNA, proteins, and membranes.[1,6,7] Furthermore, the ability of these particles to penetrate the body and cells (e.g., via fluid-phase endocytosis and caveolae) provides potential routes for the delivery of nanoparticle-associated toxic pollutants to sites where they would not normally go.[1] Nanoparticles can then behave like a vector on which hazardous compounds are concentrated.

Today, nanoparticles of SiO_2 have already been produced in very large quantities (10^2-10^3 ton/year). In China and Taiwan, silica nanoparticles are commonly used as abrasive in chemical mechanical polishing (CMP) industries for the manufacture of integrated circuits and electronic chips.[8] According to Kin et al.[9] the characteristic flow rate of rejection of these liquid effluents for each factory is about 0.42 m^3/h. The studies of several research groups[8−14] give a deep analysis of the composition of these effluents, indicating that suspensions are mainly composed of silica with an important content (1.3−8.5 g/L[11−14] which correspond to 0.05%−0.36% in volume ratio) and an average size around 100 nm. The particles present a negative charge at the surface and zeta potential of the suspension $|\zeta|$ remains lower than 30 mV. The availability of data concerning these largely produced effluents as well as the existence of commercially available products necessary for research purposes confers to SiO_2 nanoparticles the quality of interesting candidate for developing waste treatment processes.

However, nanoparticles that are different from classical solid particles by their size and specific properties due to their high surface area over volume ratio could be responsible for a low efficiency of classical water treatment processes and may demand to modify their surface physicochemical properties with some

additives such as salts or surfactants. Chuang et al.[15] have applied polyaluminum chloride (PACl) as the coagulant and cationic polyacrylamide (PAA) as the flocculant to remove nanoparticles in the CMP wastewater. Their structural researches on the nanoparticules agglomeration due to coagulation have demonstrated the interest of coagulant addition for a good recovery. Hu et al.[11] and Lien and Liu[12] have performed coagulation and flotation processes by using a cationic surfactant cetyltrimethylammonium bromide (CTAB), to address the treatment of CMP wastewater. The above studies refer to the destabilization of colloidal silica by electrostatic interaction and/or by steric interaction between nanoparticles and coagulants, but the scientific based knowledge in this process is far not enough and can be determinative for the separation process of nanoparticles. Thus, we have consequently focused our study on the understanding of the coagulation process of nano-SiO_2 by $AlCl_3$ for the following reasons: (1) the negative surface charge of silica nanoparticles favorites cations adsorption; comparing with monovalent and divalent cations, trivalent cations (Al^{3+}) as counterions have more obvious effects on neutralizing the surface charge of silica;[16] (2) although cationic surfactants and cationic polymers may be more effective for coagulation-flocculation of nano-SiO_2, their possible steric effect besides the neutralization enhance the complication of the basic research; (3) it seems that the conventional coagulation-flocculation treatments may not be adapted to the recovery of nanoscale particles because of the large amount of coagulant needed for a good recovery leading to a bulky sludge volume;[14,17] but other processes such as flotation or filtration eventually combine with coagulation for the removal of nanoparticles.[12,14,18−21]

Summarily, because the direct separation of nanoparticles would be difficult, it may be inevitable to modify their surface properties by suitable additives which usually accompany the aggregation of nanoparticles. Therefore, this basic study on the coagulation of nano-SiO_2 by $AlCl_3$ would predict some necessary information for the further study of nanoparticles separation.

2. PRELIMINARY EXPERIMENT SECTION

2.1. Materials and Methods. Klebosol 30R50 and 30R25 colloidal silica suspension were provided with an initial solid content of about 15.3% v/v (Rohm and Haas Electronic Materials, France). The stability of these manufactured suspensions were obtained through the addition of Na_2O (<0.2%) which generated anionic nano-SiO_2 surface. Particles would thus repel each other, providing a good stability to the colloid. The diluted suspensions were prepared with deionized water.

Aluminum chloride ($AlCl_3$) purchased from Santa Cruz Biotechnology, Inc. contains 99.8% of $AlCl_3$ and very small quantities of ferric chloride ($FeCl_3$), silicon tetrachloride ($SiCl_4$), and sodium chloride (NaCl).

The zeta potential of diluted suspensions was measured by electrophoresis with a Zetasizer 2000 (Malvern Instruments). pH was measured at ambient temperature with a pH-539 pH-meter (WTW) and a SenTix 41 pH-electrode and conductivities with a LF 538 conductivity meter (WTW) and a Tetracon 325 probe. Turbidity was measured with a 2100N-IS Turbidimeter (Hach).

The size of the Klebosol 30R50 and 30R25 particles were measured by transmission electron microscopy (TEM, Philips CM20 (200 kV) and JEOL 100CX) and dynamic light scattering (DLS, Nanotrac from Microtrac). The size analysis of nano-SiO_2/$AlCl_3$/water systems was done by laser diffraction

Table 1. Physicochemical Properties of the 30R50 and 30R25 Suspensions (Commercial Data and Measurements)

	30R50	30R25
particle size (nm)	$d_{datasheet} = 50^a$	$d_{datasheet} = 25^a$
	$d_{mean} = 75^b$; $d_1 \sim 40^c$, $d_2 \sim 85^c$	$d_{mean} = 30^b$; $d_1 \sim 37^c$
ζ (mV)	-35.5^d	-30^d
pH	$pH_{datasheet} = 9$ (20 °C)	$pH_{datasheet} = 9$ (20 °C)
	$pH_{mesure} = 8.81$ (23.2 °C)	$pH_{mesure} = 9$ (22.4 °C)

[a] Determined by BET. [b] Determined with Nanotrac. [c] Determined with TEM. [d] The zeta potential is measured at the concentration of 0.15% v/v with the Zetasizer 2000.

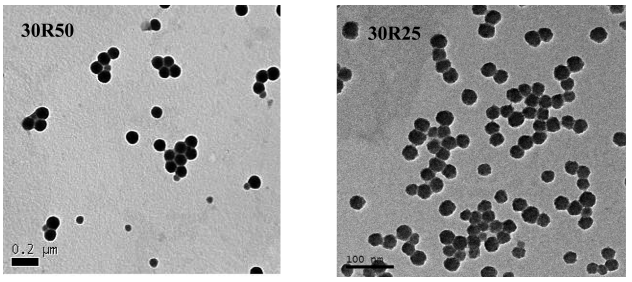

Figure 1. TEM observations of Klebosol 30R50 and 30R25 nanoparticles.

(Mastersizer 2000, Malvern Instruments) in case of the existence of aggregates.

DLS allows measuring the size below the limit of the static light diffusion and diffraction methods. The principle of this method is based on the Stokes−Einstein law which gives the size of the particles according to their Brownian diffusion coefficient and the physical properties of the medium. The size determined by DLS is a hydrodynamic diameter corresponding to the diameter of a sphere that has the same translational diffusion coefficient as the particle. The Stokes−Einstein law is valid especially for dilute suspensions, where the effect of interactions can be neglected.

Mastersizer 2000 applies laser diffraction and the full theory of Mie. The method relies on the fact that diffraction angle is inversely proportional to particle size. In the study, this method was used because the size of aggregates may not remain in the range of DLS measurement.

2.2. Characterizations of Nanoparticle Suspensions. The physicochemical characteristics of the suspensions provided by the producer and measured in the work are summarized in Table 1.

2.2.1. Characterizations of Particle Size. For Klebosol 30R50, the particles are almost spherical, but they are not monodisperse. Indeed, we can see in Figure 1 two populations: particles of about 80−85 nm in diameter and smaller ones of about 30−40 nm. A mean diameter in number was then statistically determined for each population (d_1 and d_2, Table 1). Klebosol 30R25 nanoparticles are nearly monodisperse with about 35−40 nm in diameter from Figure 1. TEM observations are important to validate other size measurements like DLS.

Figure 2 shows the particle size distribution (PSD) measured by the Nanotrac at SiO_2 concentration 0.15% (v/v); the mean diameters d are reported in Table 1. We can observe in Figure 2 that both the PSD of 30R50 and 30R25 are monomodal, while

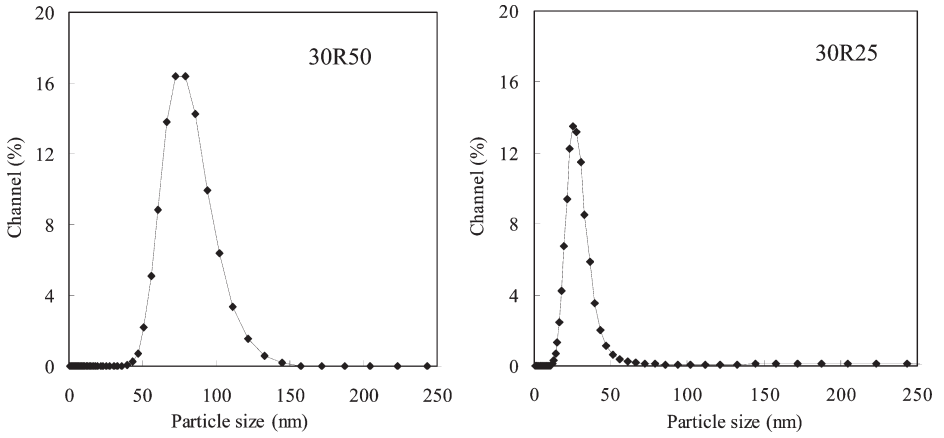

Figure 2. PSD of the Klebosol 30R50 and 30R25 suspensions measured by the Nanotrac.

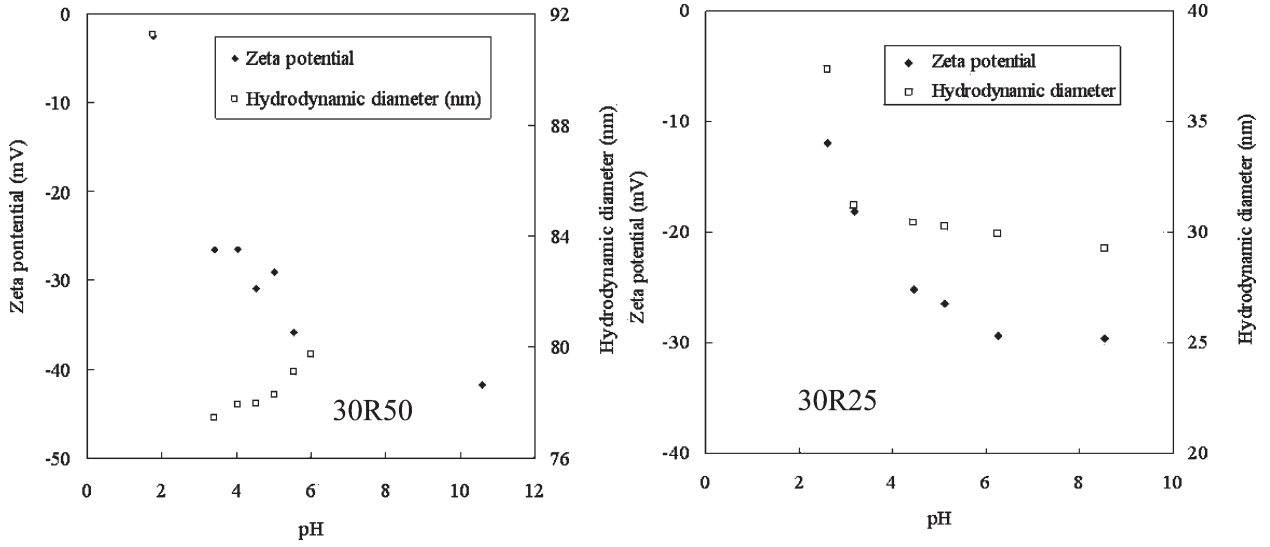

Figure 3. The zeta potential-pH profiles and hydrodynamic diameter-pH profiles for Klebosol 30R50 and 30R25 at 0.15%.

the TEM observations show two populations for 30R50. The differences can be due to the type of distribution, in number for TEM observations and in light intensity for DLS measurements, and to the fact that the distribution determined by DLS is quite wide and may incorporate the two populations observed by TEM for 30R50.

2.2.2. Analyses of Surface Charge. The zeta potential (ζ) measurements were used to provide an indication of the surface charge present on the particles when they were in aqueous suspension. For the initial silica suspensions 30R50 and 30R25, the very high and negative zeta potential measured (in absolute value $|\zeta| \geq 30$ mV in Table 1) confirmed that the stability of the system was ensured by the repulsive interaction. The results agree with those of Schwarz et al.[22] and Xing[23] who have demonstrated that the zeta potential of silica is negative at pH > 3 and $|\zeta|$ increases with increasing pH. In our study, all of the concentrations of 30R50 and 30R25 have pHs higher than 5.

The effect of pH on the zeta potential has been checked. By adding HCl or NaOH in the Klebosol 30R50 and 30R25 suspensions (see Figure 3), zeta potential can be changed with the changing pH. The isoelectric points ($\zeta \approx 0$) of silica are usually between 2 and 3,[22,24] but for 30R50 and 30R25 ($\Phi = 0.15\%$) nanosilica, no isoelectric points were found when pH $\geq$ 2.

The average size of 30R50 0.15% near the isoelectric point is about 90 nm (pH $\approx$ 2), compared with 77−79 nm for the same suspension under other pH conditions from Figure 3. For 30R25, the average size at pH $\approx$ 2 is about 37 nm, compared with about 30 nm under other pH conditions. The hydrodynamic diameters are a little greater at low pH ($\sim$2) maybe on account of the higher viscosity of water which decreases the diffusion coefficient of the particles in the medium and then increases the particles diameter calculated by the softwave based on the Stokes−Einstein law or because of the decreasing electrostatic repulsions.

It is worth noting that no aggregation of 30R50 and 30R25 were observed in all of pHs, but their zeta potentials can be modified to $|\zeta| < 10$ mV. This is different to usually reported results where $|\zeta| < 30$ often means destabilization. Figure 4 gives the possible reason of the stabilization of nanosilica at very low pH (then low $|\zeta|$). The formation of hydrogen bonds between SiO_2 nanoparticles and water could keep the suspension at a stable state. However, the stability at pH $\geq$ 3 should result from the repulsive interactions due to the negative surface charge of SiO_2 nanoparticles.

The water behavior on the silica surface may help to better understand this phenomenon. Researchers have detected by a variety of spectroscopic techniques including FTIR, Raman, and NMR that silanol (−SiOH) and siloxane ($-SiO^-$) groups are at the surface of quartz.[16] In the presence of molecular water, the silanol groups ionize, producing mobile protons that associate-dissociate with the surface to impart an electrical conductivity to the surface. As these groups dissociate, hydronium ions are produced which diffuse from the surface to develop a pH-dependent surface charge and potential. This model of bulk silica surface behaviors may help to interpret the results of nanosilica. However, it is hard to conclude on the only basis of the measured size evolution as a function of pH.

2.2.3. Turbidity Measurement. Figure 5 present that the logarithmic turbidity of 30R50 and 30R25 varies almost linearly with the logarithm of volume concentrations, which is useful for the concentration determination via turbidity measurement. For 30R50, from 0.00005% to 0.51% (turbidity from 0.5 and 622 NTU) and for 30R25, from 0.0015% and 1.53% (turbidity from 0.7 and 40 NTU), the relations between turbidity (ordinate y) and concentration (abscissa x) can be given as eqs 1 and 2

$$\lg y = 0.9033 \lg x + 3.0357; R^2 = 0.9982 \quad (1)$$

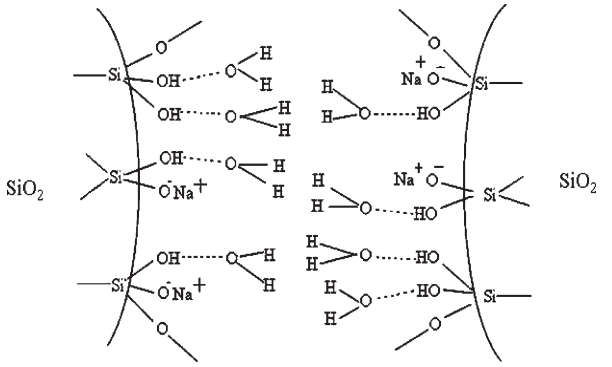

Figure 4. The possible combination of Klebosol 30R50 and 30R25 suspensions at low pH (∼2).

$$\lg y = 0.6914 \lg x + 1.4865; R^2 = 0.9988 \quad (2)$$

Thus, the turbidity can be used to indirectly analyze nanoparticles concentration after separation process. However, when there are aggregates, the turbidity values may no longer be correct to predict particle concentrations.

3. SURFACE MODIFICATION AND AGGREGATION OF SILICA NANOPARTICLES

$AlCl_3$ which has been chosen as the additive to destabilize nano-SiO_2 suspensions for the separation proposes can be hydrolyzed strongly in water. Al^{3+}, $Al(OH)^{2+}$, $Al(OH)_2^+$, $Al(OH)_{3(aq)}$, $Al(OH)_{3(s)}$, $Al(OH)_4^-$, and polymeric aluminum species would present based on the thermodynamic equilibria of possible species.[25] The pH of the solution has a significant effect on the species present, depending mainly on OH/Al ratio. The $Al(OH)_{3(s)}$ precipitate has a global positive charge for pH < 9.[25,26]

From potentiometric data and calculated concentrations, when pH is below 3, Al^{3+} is the dominant species. Above this pH, the OH^- anion is joined to the inner coordination sphere as a ligand of aluminum; the complex $Al(OH)^{2+}$ is dominantly present at the pH range 4−5. The formation of polymeric aluminum species begin approximately at pH 4.5. Above pH 8, aluminate anion $Al(OH)_4^-$ is the dominating species. Other methods to study the aluminum hydrolysis such as 27Al-NMR and mass spectrometry also show that cationic aluminum species are dominant until pH < 8.[27]

3.1. Kinetics of Nanosilica Aggregation with $AlCl_3$ at Early Stage. The study of the kinetics is useful in determining the aggregation mode, the dynamic scaling laws, and the critical coagulation concentration (CCC). Moreover, the kinetics study, usually considering coagulation at the early stage, may partially avoid the complication of different aluminum species sorption, since their hydrolyzation would last for a long period depending on the pH.

The collision of particles experience two processes during this early stage of coagulation: the reaction-limited aggregation (RLA) where a large number of collisions are required before two particles can stick together, resulting in a slow aggregation

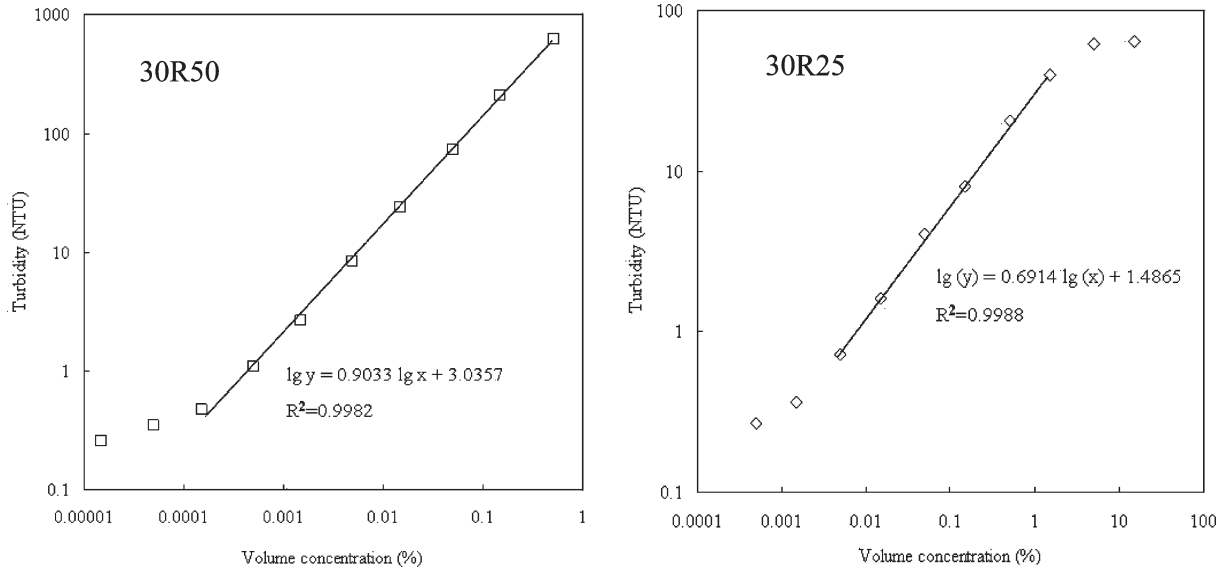

Figure 5. Experimental evolutions of turbidity with the particle concentrations for Klebosol 30R50 and 30R25 suspensions.

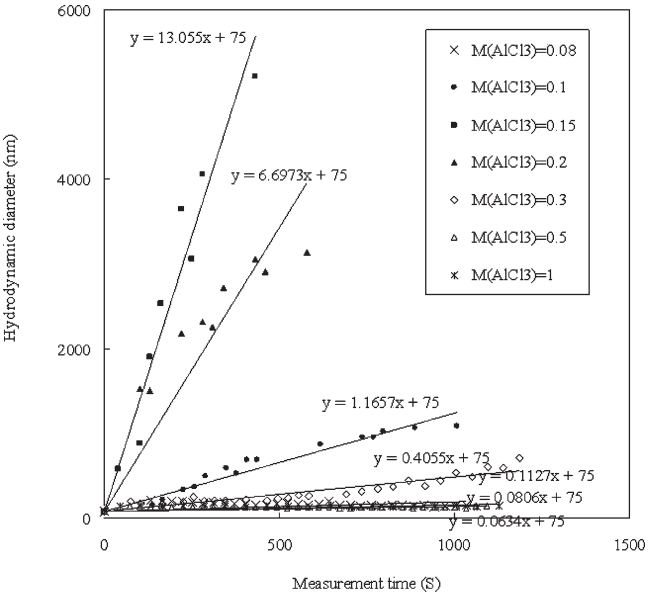

Figure 6. "Aggregation rate" versus time for 30R50 0.15% at different concentrations of $AlCl_3$ ($mmol \cdot L^{-1}$).

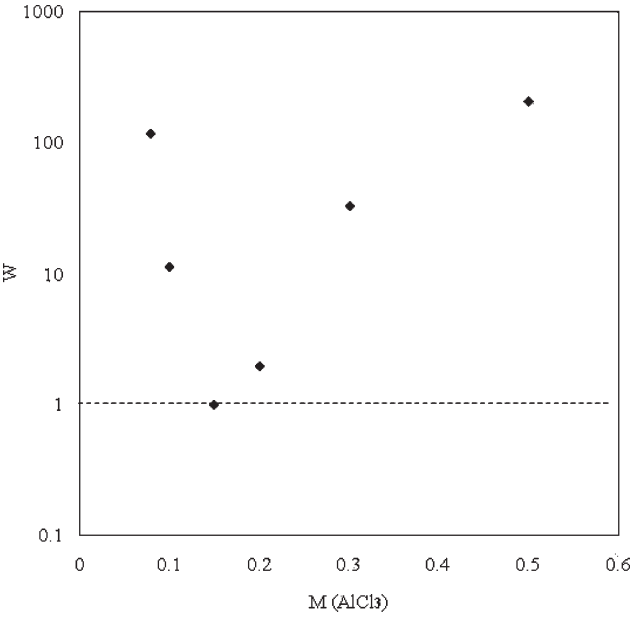

Figure 7. Stability plot for 30R50 0.15% versus concentrations of $AlCl_3$ ($mmol \cdot L^{-1}$).

rate,[28] and diffusion-limited aggregation (DLA) that the aggregation rate is limited only by the time between the collisions of the clusters due to their diffusion.[29]

In our study, the kinetics study focus on the CCC research for silica nanoparticles. By choosing a suitable concentration of $AlCl_3$ for fast particle aggregation, the stability ratio W in aggregating suspension can be obtained by

$$W = \frac{\beta_{fast}}{\beta'} \tag{3}$$

where β' is an aggregation rate in the reaction-limited regime. In this regime, an increase in the electrolyte concentration screens the surface charge of nanoparticles, leading to faster aggregation until reaching the β_{fast} in the diffusion-limited regime. The CCC is then the intersection between the extrapolations through the reaction- and diffusion-limited regimes (i.e., $W = 1$).[30]

The DLS technique that did not directly determine the aggregation rate, but rather changes in nanoparticles' sizes with time, was used to analyze the CCC by measuring the initial rate of changes in size with increasing electrolyte concentrations.[31−33] It can be demonstrated that $((\beta_{fast})/(\beta')) = ((k_{fast})/(k'))$, so the size variation with k_{fast} and k' gives W.[34] Here, k is the slope of the variation of the hydrodynamic diameter as a function of the time. For nanosilica aggregated by $AlCl_3$, the situation of CCC is more complicated due to the surface charge reverse. Large quantities of $AlCl_3$ could restabilize silica nanoparticles by the sorption of positively charged aluminum species.

3.1. CCC of Klebosol 30R50 Nanosilica. Figure 6 presents the increase rate in the hydrodynamic diameter of 30R50 (0.15%) by the addition of $AlCl_3$. The slope $k_{fast} = 13.055\ nm \cdot s^{-1}$ appears at the $M(AlCl_3) = 0.15\ mmol \cdot L^{-1}$. Other electrolyte concentrations, higher or lower than the CCC value, always cause slower "aggregation rate" k'.

Figure 7 further shows the stability ratio W of 30R50 (0.15%) depending on different concentrations of $AlCl_3$. The values of W have a tendency of first decrease and then increase. The diffusion controlled regime in Figure 7 is just a point ($W = 1$) instead of a straight line in more standard situations, indicating the continuous adsorption of aluminum species after the CCC.

Table 2. Summary of CCC and k_{fast} for 30R50 at Three Concentrations

30R50 solid content	CCC ($mmol \cdot L^{-1}$)	k_{fast} ($nm \cdot s^{-1}$)
0.15%	0.15	13.055
1.5%	1.2	16.928
5.1%	2.5	16.2

3.1.1. Concentration Effect on CCC. In order to verify and compare with the above results, other concentrations of 30R50 1.5% and 5.1% were investigated. The summary of CCC and k_{fast} at different concentrations is present in Table 2. The CCC values for these three samples seem to follow a linear dependency to the 30R50 concentrations, in agreement with the surface charge neutralization mechanism. Because of higher concentration corresponding to more nanosilica in the suspension and then more negative surface charges, more cationic ions are then needed to overcome the surface charge repulsive effect, leading to a higher CCC.

In addition, all the k_{fast} of 30R50 are found between 13 and 17 $nm \cdot s^{-1}$ (see Table 2). The k_{fast} approximation of 30R50 at different concentrations could be understood since the aggregation kinetics is Brownian diffusion-limited. Supposing nanosilica particles are indifferent to each other and sufficiently small to have negligible settling velocity, the fast rate constant β_{fast} can be based on Fick's first law with the coefficient of diffusivity estimated from the Stokes−Einstein[35,36]

$$\beta_{ij(r)} = \frac{2k_B T}{3\eta}\left(\frac{1}{r_i} + \frac{1}{r_j}\right)(r_i + r_j) \tag{4}$$

where k_B is Boltzmann's constant, T is the absolute temperature, η is the solvent viscosity, and r_i and r_j are the radii of the colloidal particles or aggregates. For a monodisperse system ($r_i = r_j$), the

rapid rate constant is reduced to

$$\beta_{(r)} = \frac{8k_BT}{3\eta} \quad (5)$$

Equations 4 and 5 indicate that β_{fast} is independent of particle concentrations. However, He et al.[37] and Tourbin and Frances[38] found that at the same ionic strength and pH, aggregation rate increased with higher particle concentration, but they also proposed that when the concentrations are not very different, there is no significant effect, especially for the diffusion-limited regime.

3.1.2. Size Effect on CCC. Klebosol nanosilica 30R25 0.15% and 1.5% were studied for the particle size effect and compared with the results of 30R50 (see Table 3). The k_{fast} of 30R25 0.15% and 1.5% are both about 30.0 nm·s^{-1}, which is about twice as fast as the k_{fast} (13−17 nm·s^{-1}) of 30R50 0.15% and 1.5%. Considering that smaller particles contribute to the faster diffusion based on Brownian motion, 30R25 nanosilica could have a faster "aggregation rate". These results indicate that the k_{fast} corresponds to the particle size rather than the particle concentration.

Through the above results of both 30R50 and 30R25, the CCC values for these samples increase almost linearly with the nanosilica concentrations. This is different from the work of Tombacz and Szekeres,[39] in which the CCC values were independent of the concentrations of montmorillonite (d > 200 nm). Since the particle size in the work is smaller, the surface nature could have a stronger influence on the CCC value. Moreover, size effect of 30R50 and 30R25 at the same concentration does not clearly show a correlation with the CCC. On the contrary, the "aggregation rates" at diffusion-limited regime marked by the slopes k_{fast} correlate with their particle sizes.

Table 3. Summary of CCC and k_{fast} for 30R50 and 30R25 at the Concentrations 0.15% and 1.5%

samples	CCC (mmol·L^{-1})	k_{fast} (nm·s^{-1})
30R50 0.15%	0.15	13.055
30R50 1.5%	1.2	16.928
30R25 0.15%	0.25	30.000
30R25 1.5%	1.5	31.394

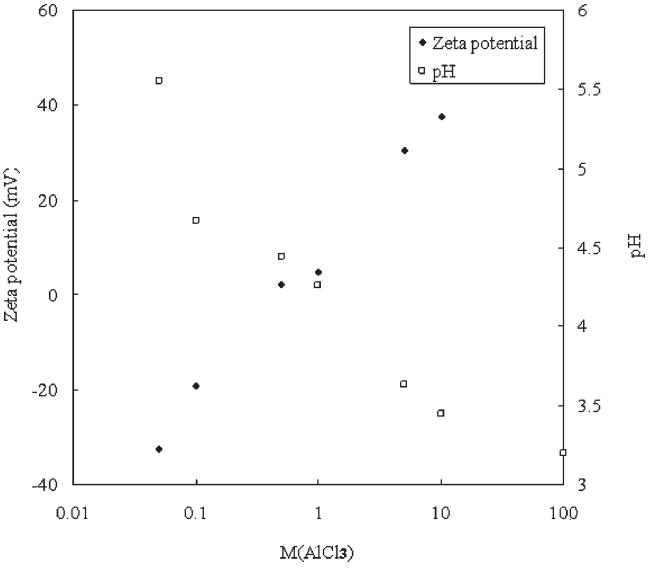

Figure 8. Zeta potential and pH profiles of the 30R50 (0.15%) at different concentrations of $AlCl_3$ (mmol·L^{-1}).

3.2. Influence of the Physicochemical Conditions on the Aggregation of Nanosilica with $AlCl_3$. The aggregation of silica nanoparticles is not only a kinetic process but also a thermodynamic process. Three concentrations of 30R50 (0.05%, 0.15%, and 0.51%) are then investigated for the aggregation results after a long time until the equilibrium.

Taking 30R50 0.15% as an example: the adsorption of $AlCl_3$ (0.05−100 mmol·L^{-1}) modifies the silica surface (zeta potentials) from negatively to positively charged (see Figure 8); and the pHs of suspensions are not more than 6, indicating cationic aluminum species dominance.

Size distributions of these samples are further shown in Figure 9. Large aggregates are obtained for $AlCl_3$ concentrations between 0.5 to 1 mmol·L^{-1}, where ζ values are near zero. M($AlCl_3$) = 0.05 and 10 mmol·L^{-1} that correspond to

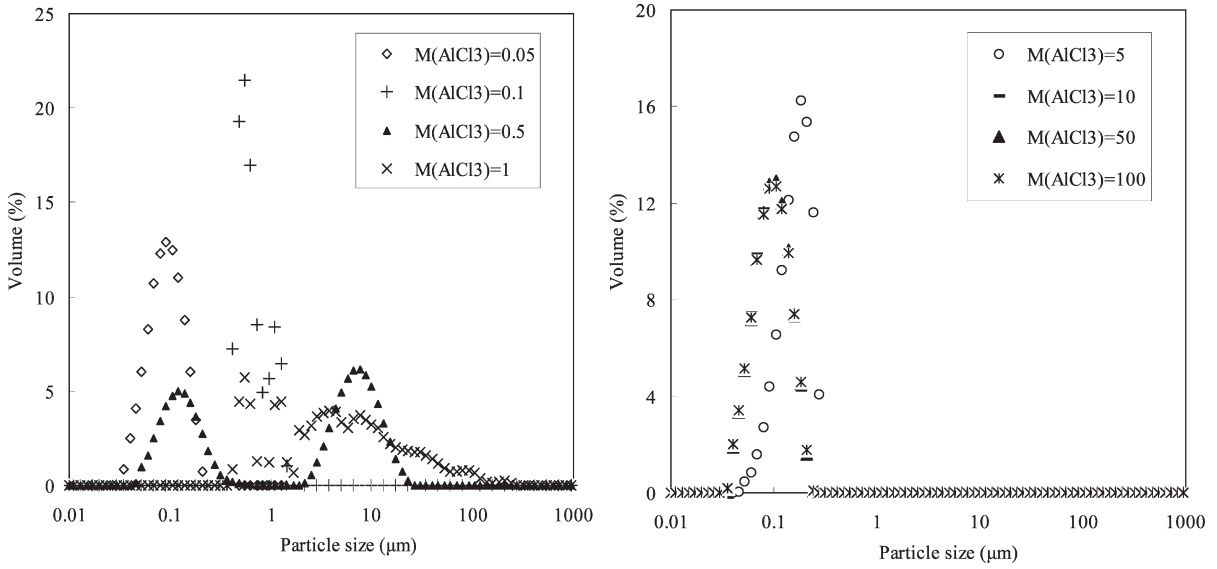

Figure 9. Particle size of the 30R50 (0.15%) with different concentrations of $AlCl_3$ (mmol·L^{-1}) analyzed by Mastersizer 2000.

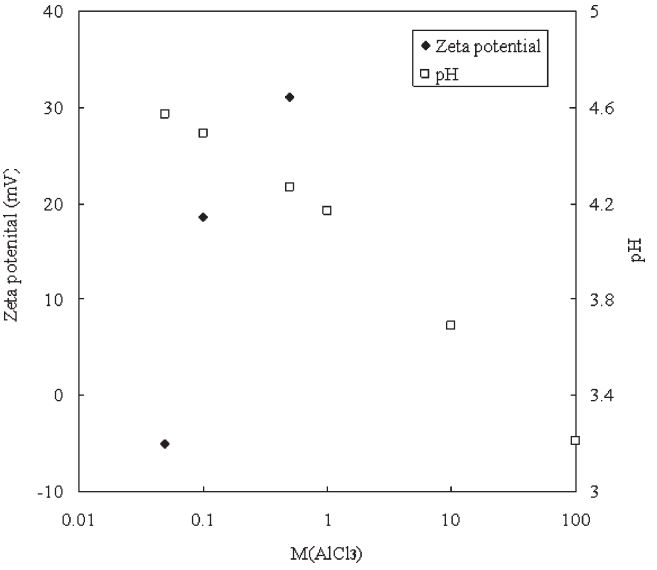

Figure 10. Zeta potential and pH profiles of the 30R50 (0.05%) at different concentrations of $AlCl_3$ (mmol·L^{-1}).

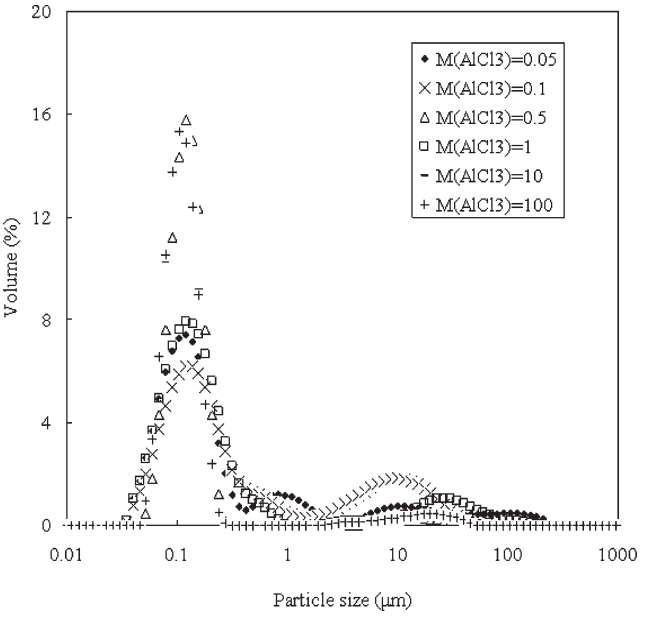

Figure 11. Particle size of the 30R50 (0.05%) at different concentrations of $AlCl_3$ (mmol·L^{-1}) analyzed by Mastersizer 2000.

$|\zeta| > 30$ mV cannot destabilize nanosilica particles. Here, ζ values of samples with $M(AlCl_3) > 50$ mmol·L^{-1} were not measured due to the excess concentrations beyond the instrument limit. Compared with $M(AlCl_3) = 10$ mmol·L^{-1} (ζ = 37.6 mV), $M(AlCl_3) > 50$ mmol·L^{-1} would correlate with higher positive ζ and then restabilize nanosilica particles by positive surface charges such as shown in Figure 9. When $M(AlCl_3) = 0.1$ mmol·L^{-1} ($\zeta = -19$ mV) and 5 mmol·L^{-1} ($\zeta = 30.4$ mV), particle sizes less increase than those near the zero point, especially for $M(AlCl_3) =$ 5 mmol·L^{-1} (ζ = 30.4 mV). Furthermore, for 30R50 0.15%, the largest aggregates from $AlCl_3$ reached about 100 μm, but most of them were about 10 μm.

It can be noted that at long time equilibrium the aggregates of 30R50 0.15% begin to be observed at the $AlCl_3$ concentration 0.1 mmol·L^{-1}, which is similar to the CCC determined at the early agglomeration stage. However, this may not be always true for other concentrations of 30R50. As the aggregation of 30R50 0.15% can be well explained by the surface potential measurement and the charge neutralization mechanism, 30R50 0.05% and 0.51% were further studied for the particle concentration effect on aggregation.

3.2.1. Effect of Particle Concentration. For 30R50 0.05% in Figure 10, when $M(AlCl_3) > 1$ mmol·L^{-1}, ζ values could not be correctly analyzed, but they are expected to be more than 30 mV and could restabilize silica particles. $M(AlCl_3) = 0.05$ and 0.1 mmol·L^{-1} which correspond to $|\zeta| < 20$ mV should cause aggregation, but size distributions in Figure 11 only present a few aggregates. This may be due to the very low concentration (0.05%) of silica nanoparticles. Otherwise, the interpretation might be the presence of a "hairy layer" (see Figure 12) consisting of polysilicilic acid on the silica particle surface at low/mid pH and relatively high ionic strength. Water molecules could dissolve or diffuse into and swell the silica,[35] possibly causing the "hairy layer". Hence, repulsion may be attributed to the strain of elastic deformation or to steric repulsion of polysilicilic acid chains suggested to constitute the gel layer. Existence of such a layer has been suggested on the basis of direct force measurements or simulation between silica particles.[34,40−42]

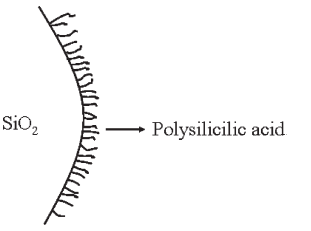

Figure 12. The schematic of the "hairy layer" on the silica particle surface.

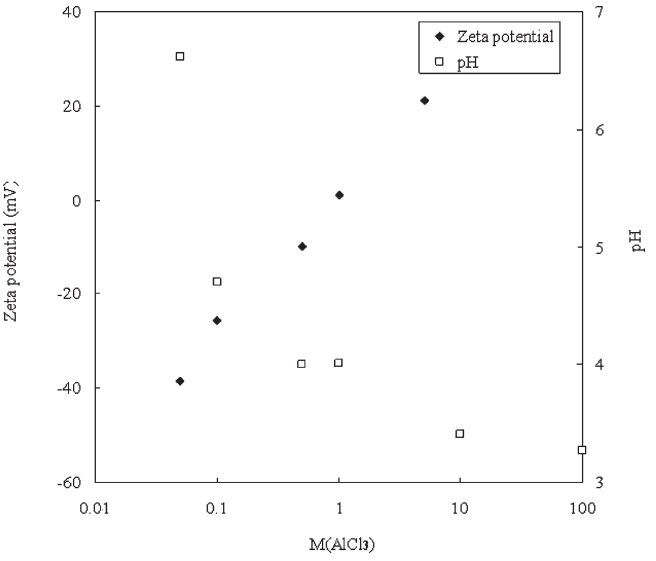

Figure 13. Zeta potential and pH profiles of the 30R50 (0.51%) at different concentrations of $AlCl_3$ (mmol·L^{-1}).

For 30R50 0.51% from Figure 13, ζ values ($|\zeta| < 30$ mV) suggest that the aggregation should happen for $M(AlCl_3)$ between

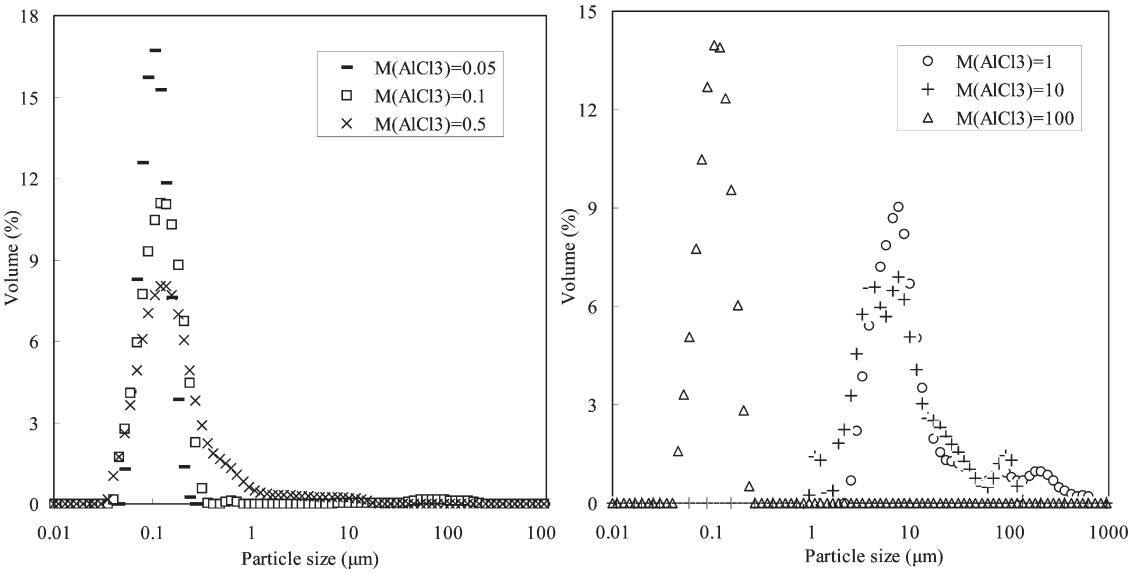

Figure 14. Particle size of the 30R50 (0.51%) at different concentrations of $AlCl_3$ ($mmol \cdot L^{-1}$) analyzed by Mastersizer 2000.

Table 4. Turbidity Values of 30R50 (0.05%, 0.15%, 0.51%) after Aggregation

$M(AlCl_3)$ ($mmol \cdot L^{-1}$)	0	0.05	0.1	0.5	1	10	100
turbidity of 30R50 0.05% (NTU)	61.9	70	97.6	46.6	113	67.8	85.4
turbidity of 30R50 0.15% (NTU)	171	218	1027	1.3	0.6	250	219
turbidity of 30R50 0.51% (NTU)	542	798	1059	876	0.4	0.4	732

0.1 to 10 $mmol \cdot L^{-1}$. Contrarily, the size distributions in Figure 14 only show aggregates at $M(AlCl_3)$ = 1 and 10 $mmol \cdot L^{-1}$. The stability of Klebosol 30R50 0.51% at $M(AlCl_3)$ = 0.1 and 0.5 $mmol \cdot L^{-1}$ may also result from the repulsion of hairy structure on silica surface. Similar to 30R50 0.15%, a majority of aggregates have a size of about 10 μm.

3.2.2. Sedimentation of Silica Aggregates. Turbidity of these samples was measured to check if silica nanoparticles could be removed just from sedimentation after aggregation. After 2 weeks of aggregation and sedimentation at rest, the aggregates were laid down at the bottom of the vials and the supernatant liquid was analyzed.

From Table 4, turbidity values of 30R50 0.05% with different concentrations of $AlCl_3$ show no significant changes. This agrees with the size distribution measurements of 30R50 0.05% with $AlCl_3$ in Figure 11, where most of the nanoparticles remain at about 0.1 μm. However, for 30R50 0.15% (1 $mmol \cdot L^{-1}$ $AlCl_3$) and 30R50 0.51% (1 and 10 $mmol \cdot L^{-1}$ $AlCl_3$), it was possible to remove more than 99% of the turbidity.

It can also be observed in Table 4 that the turbidity value of 30R50 0.15% with 0.1 $mmol \cdot L^{-1}$ $AlCl_3$ much increases after 2 weeks. Referring to Figure 9, size distribution of this sample is about 1 μm, indicating that small aggregates dispersed in the suspension which then enhanced the turbidity. Other concentrations of $AlCl_3$ (0.05, 10, and 100 $mmol \cdot L^{-1}$) with 30R50 0.15% have nearly the same turbidity as 30R50 0.15% itself. Their size distributions in Figure 9 show little change as well.

After a series of tests on the aggregation behavior from three concentrations of nanosilica 30R50, only 0.15% could be well explicated by the screen of electrostatic repulsion from the DLVO theory. There is certainly another force between these colloidal particles. To better understand the aggregation behavior and the particle size effect, nanosilica 30R25 was also studied as presented subsequently.

Table 5. Zeta Potential and pH of 30R25 0.15% with $AlCl_3$

$M(AlCl_3)$ ($mmol \cdot L^{-1}$)	0.1	0.5	0.6	1	5
zeta potential (mV)	−28	−0.29	6.9	13.2	44.3
pH	4.78	3.81	3.5	3.39	3.64

3.2.3. Effect of Particle Size. Comparison between the total surface (S) of 30R25 and 30R50 at the same volume concentration (%), S_{30R25} is about 2 times as large as S_{30R50} (2 being the ratio between the radii of 30R50 and 30R25). This is because the number of particles N_{30R25} equals $((N_{30R50} \cdot r_{30R50}^3)/(r_{30R25}^3))$ (r is the radius of nanoparticles) at the same volume concentration. The total surface S_{30R25} equals $N_{30R25} \cdot C \cdot r_{30R25}^2$ (C is the constant). Thus

$$\frac{S_{30R25}}{S_{30R50}} = \frac{N_{30R25} \cdot C \cdot r_{30R25}^2}{N_{30R50} \cdot C \cdot r_{30R50}^2} = \frac{r_{30R50}}{r_{30R25}} \approx 2 \quad (6)$$

As most of the atoms are exposed to the nanoparticles surface, the change in surface properties caused by the reduction in diameter might modify their behaviors during the aggregation. 30R25 0.15% is studied to compare with the aggregation of 30R50 0.15% for the size effect.

Table 5 gives the zeta potential and pH values of 30R25 0.15% with different concentrations of $AlCl_3$, in which the isoelectric point appears at about $M(AlCl_3)$ = 0.5 $mmol \cdot L^{-1}$. Noted that the isoelectric point for 30R50 0.15% in Figure 8 is about $M(AlCl_3)$ = 0.5 $mmol \cdot L^{-1}$ as well, but it has a smaller total surface area and then less silanol and siloxane (negative charges) on the surface due to their larger diameter. This should result in the isoelectric point of 30R25 0.15% to be found at larger concentration of $AlCl_3$ than in the case of 30R50 0.15%. It is difficult to explain the abnormity. The possible reason may be the complicated formation of nanosilica and aluminum species or the different aggregation mechanisms. In addition, the initial

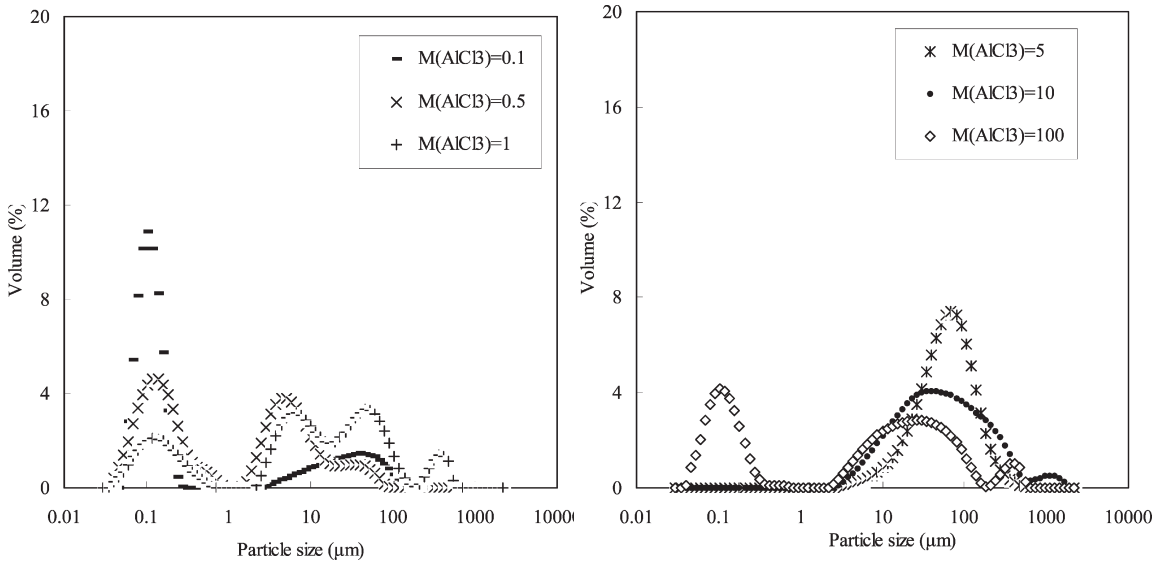

Figure 15. Particle size of the 30R25 (0.15%) at different concentrations of $AlCl_3$ ($mmol \cdot L^{-1}$) analyzed by Mastersizer 2000.

compositions of 30R50 and 30R25 could be different, because the quantity of Na_2O in these products is actually unknown; this is probably the main reason of the abnormity.

The size distributions of these samples are shown in Figure 15. All of them presented aggregates whatever their ζ values. For $M(AlCl_3)$ = 5 and 10 $mmol \cdot L^{-1}$, few nanoparticles of 30R25 are detected. The large aggregates can increase until 1000 μm, but most of them are smaller ($\leq$1000 μm).

Generally, coagulants based on hydrolyzing metal salts such as $AlCl_3$ could form various cationic species. These cationic species would be adsorbed by negatively charged particles and lead to charge reduction. At low concentrations, charge neutralization is a possible mechanism of particle destabilization, but at a ionic strength sufficiently high, $Al(OH)_3$ could form and colloidal particles can be enmeshed in these precipitates.[43,44] As particles of 30R25 are smaller than those of 30R50, they are more likely to be captured by the sweep of $Al(OH)_3$ precipitates. This may be one reason for the aggregates of 30R25 0.15% formed at high $M(AlCl_3)$ and high positive ζ.

So far, the aggregation behavior for three particle concentrations (0.05%, 0.15%, 0.51%) and two particle sizes (30R50 and 30R25) have been discussed and compared. Since many factors such as particle concentration, particle size, electrolyte concentration, pH of the solution, particle surface properties... would all affect the aggregation; it is difficult to correlate all the parameters and to explain the process by one given mechanism.

For Klebosol 30R50, the aggregation of silica nanoparticles could be mainly due to the charge neutralization; while in relatively high ions concentration, the possible hairy layer formed on silica surface may contribute to particles stability at $|\zeta| \geq$ 30 mV. The sweep flocculation by $Al(OH)_3$ precipitate might be the reason for 30R25 particles aggregation at sufficiently high $M(AlCl_3)$.

4. CONCLUSION AND PROSPECT

After a review of some papers dealing with the potential hazards of nanoparticles released in the water resources, our work was focused on the separation of nanoparticles from water. Two sizes of nanosilica (Klebosol 30R50 and 30R25) have been chosen as the representatives. Their properties including size, surface charge, and turbidity have been characterized. The negative surface charge ($|\zeta| \geq$ 30 mV) insures these particles stable in water, and their small sizes ($d_{30R50} \approx$ 75 nm and $d_{30R25} \approx$ 30 nm from DLS) bring difficulties to the further separation. It was then inevitable to modify their surface physicochemical properties for the separation propose, and keeping this process as "green" as possible is our expectation.

Through the aggregation study of silica nanoparticles by $AlCl_3$, large aggregates can be obtained and further removed by sedimentation. In some cases, the turbidity removal can reach more than 99%, but this process usually takes a long time ($\approx$2 weeks).

The kinetics study would be helpful to not only better understand the aggregation but also to select operation parameters for the further separation. For this purpose, the CCC study of silica nanoparticles is investigated by adding different concentrations of $AlCl_3$. Particle concentrations seem to have a linear relation with their CCC values. Higher particle concentrations which correspond to more particles in suspensions require more cations to neutralize and then would result in higher CCC. However, for different concentrations of nanosilica (0.15%, 1.5%, and 5.1%), the rates of change in size for both 30R50 and 30R25 in the diffusion-limited regime (k_{fast}) are nearly the same.

The comparison of the CCC values between 30R50 and 30R25 at the same concentration (0.15% and 1.5%) is also reported. Although the DLVO theory predicts the smaller the particle size, the more susceptible to aggregate, the experimental results are different from the prediction. The surface properties have to be taken into consideration when particles dimension is in the nano range. A larger surface area for 30R25 would bring more negatively charged groups on its surface than 30R50, indicating a large amount of cations required to neutralize them. These two effects reversely work at the same time, so the particle size effect on the CCC may be counteracted. Nevertheless, the rate of change in size k_{fast} of 30R25 is almost twice as high as k_{fast} of 30R50.

It has to be noted that the charge neutralization mechanism dominate in the early stage of aggregation in the CCC research, but other mechanisms such as a possible "hairy layer" for 30R50

at relatively high ionic strength and sweep flocculation based on the precipitation of $Al(OH)_3$ for 30R25 could overcome the charge neutralization effect at the thermodynamic equilibrium.

Summarily, the kinetics and thermodynamics researches of nanosilica aggregation would provide scientific knowledge for the further separation study. Although insteading $AlCl_3$ by polyaluminum chloride are expected to increase the separation efficiency of aggregation, it has a defect of bulking sludge. Contrarily, the separation of nanoparticles by flotation or filtration which seem to be eco-friendly might be inefficient.[31] Therefore, combining coagulation and flotation/filtration would be the possible future research direction.

AUTHOR INFORMATION

Corresponding Author

*E-mail: pascal.guiraud@insa-toulouse.fr.

Present Addresses

#Laboratoire de Génie Chimique, 4 Allée Emile Monso, 31432 Toulouse, France.

ACKNOWLEDGMENT

The authors are grateful to CNRS (Projet PEPS), Région Midi Pyrénées, and French National Research Agency (NANOSEP, ANR-08-ECOT-009) for financial support. We acknowledge China scholarship council (CSC) for the scholarship.

REFERENCES

(1) Moore, M. N. Do Nanoparticles Present Ecotoxicological Risks for the Health of the Aquatic Environment?. *Environ. Int.* **2006**, *32*, 967.

(2) Daughton, C. G. Non-regulated Water Contaminants: Emerging Research. *Environ. Impact Assess.* **2004**, *24*, 711.

(3) Chalupa, D. C.; Morrow, P. E.; Oberdörster, G.; Utell, M. J.; Frampton, M. W. Ultrafine Particle Deposition in Subjects with Asthma. *Environ. Health Perspect.* **2004**, *112*, 679.

(4) Oberdüorster, G. Toxicology of Ultrafine Particles; in Vivo Studies. *Philos. Trans. R. Soc., A* **2000**, *358*, 2719.

(5) Reijnders, L. Cleaner Nanotechnology and Hazard Reduction of Manufactured Nanoparticles. *J. Cleaner Prod.* **2006**, *14*, 124.

(6) Brown, D. M.; Wilson, M. R.; MacNee, W.; Stone, V.; Donaldson, K. Size Dependent Proinammatory Effects of Ultrafine Polystyrene Particles: A Role for Surface Area and Oxidative Stress in the Enhanced Activity of Ultrafines. *Toxicol. Appl. Pharmacol.* **2001**, *175*, 191.

(7) Cheng, X. K.; Kan, A. T.; Tomosom, M. B. Naphthalene Adsorption and Desorption from Aqueous C_{60} Fullerene. *J. Chem. Eng. Data* **2004**, *49*, 675.

(8) Chin, C. J.; Chen, P. W.; Wang, L. J. Removal of Nanoparticles from CMP Wastewater by Magnetic Seeding Aggregation. *Chemosphere* **2006**, *63*, 1809.

(9) Kin, K. T.; Tang, H. S.; Chan, S. F.; Raghavan, S.; Martinez, S. Treatment of Chemical-mechanical Planarization Wastes by Electrocoagulation/Electro-Fenton Method. *IEEE T. Semiconduct. M.* **2006**, *19*, 208.

(10) Lai, C. L.; Lin, S. H. Electrocoagulation of Chemical Mechanical Polishing (CMP) Wastewater from Semiconductor Fabrication. *Chem. Eng. J.* **2003**, *95*, 205.

(11) Hu, C. Y.; Lo, S. L.; Li, C. M.; Kuan, W. H. Treating Chemical Mechanical Polishing (CMP) wastewater by Electro-coagulation-flotation. *Water Sci. Technol.* **2005**, *120*, 15.

(12) Lien, C. Y.; Liu, J. C. Treatment of Polishing Wastewater from semiconductor Manufacturer by Dispersed Air Flotation. *J. Environ. Eng.* **2006**, *132*, 51.

(13) Yang, G. C. C.; Tsai, C. M. T. Performance Evaluation of a Simultaneous Electrocoagulation and Electrofiltration Module for the Treatment of Cu-CMP and Oxide-CMP Wastewaters. *J. Membr. Sci.* **2006**, *286*, 36.

(14) Tsai, J. C.; Kumar, M.; Chen, S. Y.; Lin, J. G. Nano-bubble Flotation Technology with Coagulation Process for the Cost-effective Treatment of Chemical Mechanical Polishing Wastewater. *Sep. Purif. Technol.* **2007**, *58*, 61.

(15) Chuang, S. H.; Chang, T. C.; Ouyang, C. F.; Leu, J. M. Colloidal Silica Removal in Coagulation Processes for Wastewater Reuse in a High-tech Industrial Park. *Water Sci. Technol.* **2007**, *55*, 187.

(16) Papirer, E. *Adsorption on Silica Surfaces*; Marcel Dekker Inc.: New York, 2000.

(17) Chuang, T. C.; Huang, C. J.; Liu, J. C. Treatment of Semiconductor Wastewater by Dissolved Air Flotation. *J. Environ. Eng.* **2002**, *128*, 10.

(18) Huang, C.; Jiang, W.; Chen, C. Nano Silica Removal from IC Wasterwater by Pre-coagulation and Microfiltration. *Water Sci. Technol.* **2004**, *50*, 133.

(19) Yang, G. C. C.; Li, C. J. Electrofiltration of Silica Nanoparticle—containing Wastewater Using Tubular Ceramic Membranes. *Sep. Purif. Technol.* **2007**, *58*, 159.

(20) Yang, G. C. C.; Yang, T. Y.; Tsai, S. H. Crossow Electromicrofiltration of Oxide-CMP Wastewater. *Water Res.* **2003**, *37*, 785.

(21) Lin, Y. T.; Sung, M.; Sanders, P. F.; Marinucci, A.; Huang, C. P. Separation of Nanosized Colloidal Particles Using Cross-flow Electrofiltration. *Sep. Purif. Technol.* **2007**, *58*, 138.

(22) Schwarz, S.; Lunkwitz, K.; Keβler, B.; Spiegler, U.; Killmann, E.; Jaeger, W. Adsorption and Stability of Colloidal Silica. *Colloid Surf., A* **2000**, *163*, 17.

(23) Xing, Y. Study on Stability of Nano-SiO_2 Aqueous Suspension. *Paint & Coatings Industry* **2006**, *36*, 58.

(24) Sokolov, I.; Ong, Q. K.; Shodiev, H.; Chechik, N.; James, D.; Oliver, M. AFM Study of Forces Between Silica, Silicon Nitride and Polyurethane Pads. *J. Colloid Interface Sci.* **2006**, *300*, 475.

(25) Han, M. Y.; Kim, M. K.; Shin, M. S. Generation of a Positively Charged Bubble and its Possible Mechanism of Formation. *J. Water Supply Res. T.* **2006**, *55*, 471.

(26) Li, C.; Somasundaran, P. Reversal of Bubble Charge in Multivalent Inorganic Salt Solutions — Effect of Aluminum. *J. Colloid Interface Sci.* **1992**, *148*, 587.

(27) Rämö, J. *The Hydrolysis of Aluminium, A Mass Spectrometric Study*. PhD Thesis, University of Oulu, 2007.

(28) Lin, M. Y.; Lindsay, H. M.; Weitz, D. A.; Klein, R.; Ball, R. C.; Meakin, P. Universal Diffusion-limited Colloid Aggregation. *J. Phys.: Condens. Matter* **1990**, *2*, 3090.

(29) Elaissari, A.; Pefferkorn, E. Aggregation Modes of Colloids in the Presence of Block Copolymer Micelles. *J. Colloid Interface Sci.* **1990**, *143*, 343.

(30) Hsu, J. P.; Liu, B. T. Stability of Colloidal Dispersions: Charge Regulation/Adsorption Model. *Langmuir* **1999**, *15*, 5219.

(31) Kobayashi, M.; Juillerat, F.; Galletto, P.; Bowen, P.; Borkovec, M. Aggregation and Charging of Colloidal Silica Particles: Effect of Particle Size. *Langmuir* **2005**, *21*, 5761.

(32) Thomas, Y.; Wan, J.; Tokunaga, T. Kinetic stability of hematite nanoparticles: the effect of particle sizes. *J. Nanopart. Res.* **2008**, *10*, 321.

(33) Buettner, K. M.; Rinciog, C. I.; Mylon, S. E. Aggregation kinetics of cerium oxide nanoparticles in monovalent and divalent electrolytes. *Colloids Surf., A* **2010**, *366*, 74.

(34) Liu, Y. *Elimination de Nanoparticules d'Effluents Liquides*. PhD Thesis, Université de Toulouse, 2010.

(35) Amal, R.; Coury, J. R.; Raper, J. A.; Walsh, W. P.; Waite, T. D. Structure and Kinetics of Aggregating Colloidal Haematite. *Colloids Surf.* **1990**, *46*, 1.

(36) Gardner, K. H.; Theis, T. L. A Unified Kinetic Model for Particle Aggregation. *J. Colloid Interface Sci.* **1995**, *180*, 162.

(37) He, Y. T.; Wan, J.; Tokunaga, T. Kinetic Stability of Hematite Nanoparticles: the Effect of Particle Size. *J. Nanopart. Res.* **2008**, *10*, 321.

(38) Tourbin, M.; Frances, C. Monitoring of the Aggregation Process of Dense Colloidal Silica Suspensions in Astirred Tank by Acoustic Spectroscopy. *Powder Technol.* **2009**, *190*, 25.

(39) Tombacz, E.; Szekeres, M. Colloidal Behavior of Aqueous Montmorillonite Suspensions: the Specific Role of pH in the Presence of Indifferent Electrolytes. *Appl. Clay Sci.* **2004**, *27*, 75.

(40) Atkins, D. T.; Ninham, B. W. Surface and Structural Forces Measured Between Silica Surfaces in 1, 2-Ethanediol. *Colloids Surf., A* **1997**, *129−130*, 23.

(41) Kobayashi, M.; Juillerat, F.; Galletto, P.; Bowen, P.; Borkovec, M. Aggregation and Charging of Colloidal Silica Particles: Effect of Particle Size. *Langmuir* **2005**, *21*, 5761.

(42) Kobayashi, M.; Skarba, M.; Galletto, P.; Cakara, D.; Borkovec, M. Effects of Heat Treatment on the Aggregation and Charging of Stöber-type Silica. *J. Colloid Interface Sci.* **2005**, *292*, 147.

(43) Wu, X.; Ge, X.; Wang, D.; Tang, H. Distinct Coagulation Mechanism and Model Between Alum and High Al_{13}-PACl. *Colloids Surf., A* **2007**, *305*, 89.

(44) Li, T.; Zhu, Z.; Wang, D.; Yao, C.; Tang, H. Characterization of Floc Size, Strength and Structure Under Various Coagulation Mechanisms. *Powder Technol.* **2006**, *168*, 104.